Diisobutylene Maleic Acid Copolymer (DIBMA) Lipid Particle: A "Stealth" Membrane Mimetic for Neutron Scattering

Rong Guo, [1, 2] Jacob Sumner,[1] Shuo Qian [1]*

[1]Neutron Scattering Division, Oak Ridge National Laboratory, Oak Ridge, TN 37831, U.S.A.

[2]Grinnell College, Grinnell, IA U.S.A.

Corresponding Author

* Shuo Qian; Oak Ridge National Laboratory; PO Box 2008; MS-6393; Oak Ridge, TN 37831;

email: qians@ornl.gov; phone: 865-241-1934

Notes

The authors declare no competing financial interests.

Abstract:

The study of membrane protein remains challenging, especially in a native membrane environment. Recently, major progress has been made in using maleic acid copolymers such as styrene maleic acid to purify and study membrane proteins directly with native lipids associated with the membrane. Additional maleic acid copolymer membrane mimetic systems are being developed and found to have improved spectroscopic properties and pH stability. Diisobutylene maleic acid (DIBMA) has been shown to solubilize and purify membrane proteins from a native lipid bilayer into nanodiscs without the need for a detergent. To explore DIBMA lipid particles as a suitable membrane mimetic system for neutron scattering studies of membrane proteins, we measured and determined the contrast matching point of DIBMA to be ~12% (v/v) D_2O—similar to that of most protiated lipid molecules, but distinct from that of regular protiated proteins, providing a natural contrast for separating neutron scattering signals. Using SANS contrast variation, we demonstrated that the scattering from the whole lipid particle can be annihilated. Further, the lipid part of the particle shows a well-defined discoidal shape with DIBMA contrast matched. These results demonstrate that the DIBMA lipid particle is an outstanding “stealth” membrane mimetic for membrane proteins.

Introduction:

Membrane proteins represent around 23% of known genes[1] and comprise more than 60% of current drug targets[2]. However, studying membrane proteins remains a challenge because of their insolubility and instability in aqueous solutions. Thus, an effective membrane-mimetic system is necessary to conduct structural and functional studies of membrane proteins in solution. Detergents are commonly used to solubilize membrane proteins; however, detergent molecules cannot reproduce the physical and chemical properties of typical biomembranes. Other amphiphilic agents and techniques are being developed for extracting and studying membrane proteins in more effective membrane-mimetic environments. Recent developments have included systems such as bicelles[3], amphipathic polymers such as amphipol[4], membrane scaffolding protein (MSP) lipid nanodiscs[5], and maleic acid copolymer lipid nanodisc/particles[6–9]. Among them, lipid nanodiscs and lipid particles assembled by MSP or maleic acid copolymers are the most versatile and promising systems. They usually contain a patch of phospholipid bilayer with a lipid hydrophobic region shielded by amphipathic molecules such as peptide or polymer—are tunable in lipid composition to the specific needs of different membrane proteins, e.g., different ratios of charged and neutral lipids, and lipids with different chain lengths or saturations. They can provide an environment that more closely mimics a native membrane. Their size is also tunable to satisfy a plethora of membrane protein complexes, allowing for studies in solution using many biophysical tools, and structural techniques such as cryo-electron microscopy, nuclear magnetic resonance, and small-angle X-ray and neutron scattering (SAXS and SANS).

Lipid-particle–forming synthetic amphiphilic copolymers with alternating maleic acids, such as styrene-maleic acid (SMA) in various styrene/maleic acid ratios (e.g., 3:1, 2:1),

diisobutylene maleic acid (DIBMA)[8,10], and styrene maleimide (SMI)[9] have recently been quite successful in solubilizing membrane proteins. For instance, in various cases, SMA copolymers were found to directly extract membrane proteins and their associated lipids to form SMA-stabilized lipid particles, or SMALPs. The discovery of SMALPs provides opportunities for the study of membrane proteins in their native membranes[11–14]. Yet, there are some limitations to SMALPs: they are not compatible with far-ultraviolet (UV) spectroscopy and are sensitive to divalent cations and neutral to acidic pH. It has been shown that SMA, especially SMA(3:1), affects the lipid chain order and consequently might influence the functions of embedded membrane proteins. The DIBMA copolymer has diisobutylene as the alternating moiety with maleic acid at a ratio of 1:1 [Scheme. 1]. It has been found to solubilize cell membranes while having a minor impact on lipid chain order and dynamics, and it is compatible with far-UV spectroscopy[8]. This polymer works well at different pH values, with both monovalent and divalent cations[15]. Therefore, DIBMA lipid particles (DIBMALPs) provide an alternative platform to study membrane proteins in diverse conditions.[10]

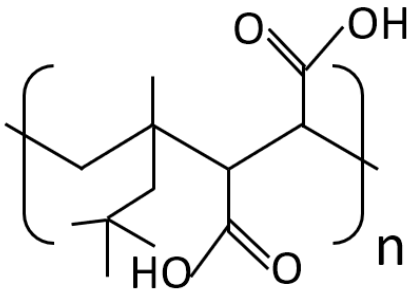

Scheme. 1. Chemical structure of DIBMA

To better understand the membrane solubilization properties of DIBMA and provide a structural framework for its application in lipid particle, we studied DIBMA and DIBMALP with SANS to understand the lipid particle morphology Small angle scattering techniques provide

straightforward structural information such as overall dimensions, shape, and molecular organization in solution over length scales ranging from a few nanometers to hundreds of nanometers. They have been widely used for understanding structures of many polymers and biomacromolecules, including lipids and membrane proteins in aqueous solution[16–18]. Understanding DIBMALP morphologies will aid in developing better strategies for solubilizing membranes. SANS techniques also benefit from the application of DIBMALPs to the solubilization of membrane proteins. DIBMA, which is similar to SMA in the direct extraction of membrane proteins and native membranes, is a valuable membrane mimic for membrane protein studies in solution by small-angle scattering.

From our SANS contrast variation experiment, the contrast matching point (CMP) of DIBMA was found to be ~12% (v/v) D_2O, similar to that of most protiated lipid molecules[18]. We demonstrated that the scattering of a whole DIBMALP can be suppressed with a 12% D_2O buffer. Typical protiated membrane proteins, with CMPs of around 42% D_2O, can be studied without the scattering of DIBMALPs contributing to the signal. Here, we demonstrated that a DIBMALP is an ideal "stealth" membrane mimic system for SANS studies, in which the neutron scattering length density of copolymer and lipid are matched by aqueous buffer of the same neutron scattering length density.[19,20]21 Thus, a membrane protein embedded within can be studied without seeing its membrane mimetic environment.

Material and Methods

Materials and Sample Preparation

DIBMA was purchased from Anatrace [part number BMA101]. It was purified from Sokalan CP9 (BASF) with diisobutylene to a maleic acid ratio of 1:1. The lipids1,2-dimyristoyl-

sn-glycero-3-phosphocholine (DMPC), 1,2-dimyristoyl-d54-sn-glycero-3-phosphocholine (d54-DMPC), were purchased from Avanti Polar Lipids Inc. (Alabaster, AL, USA). The materials were used without any further purification. DIBMA was dissolved as a 10 mM stock solution in Tris buffers (50 mM Tris, 50 or 100 or 200 mM NaCl, at pH 7.5). The stock solution was filtered with a 0.22 μm size filter. The desired concentrations of 5 mM, 2 mM, and 1 mM DIBMA solutions were obtained by diluting 10 mM stock solution with desired buffers.

The lipid solutions (1% w/w) were prepared by dissolving the lipids of interest (DMPC or mixture of DMPC/DMPG) in the same buffer used for the DIBMA solution to be titrated. The suspension was vortexed, was run through three freeze-thaw cycles, and underwent 30-fold extrusion at 35°C to ensure the formation of large unilamellar vesicles above the lipid liquid phase transition temperature (DMPC phase transition temperature ~23°C). Afterward, lipid vesicles and DIBMA were mixed in appropriate ratios and incubated to form DIBMALPs for at least 1 hour before experiments.

Small Angle Neutron Scattering

SANS measurements were performed at the EQ-SANS instrument (BL-6) of the Spallation Neutron Source (SNS) and the Bio-SANS instrument of the High Flux Isotope Reactor (HFIR) at Oak Ridge National Laboratory (USA)[22]. A q-range of ~0.0055 to 0.685 $Å^{-1}$ at the EQ-SANS was provided from two instrument configurations: sample-to-detector distance of 4 m (wavelength band ~10–13 Å) and 2.5 m (wavelength band ~2.6–6 Å). At Bio-SANS, the q-range ~0.007 to 0.6 $Å^{-1}$ was provided by a single instrument configuration with a small-angle detector at a sample-to-detector distance of 7 m and a wide-angle detector at 1.13 m. The sample aperture was set to 10 mm in diameter at both instruments. The samples were loaded in a 1 mm beam path quartz banjo cell (Hellma Inc., Plainview, NY, USA). The sample temperature was

controlled by a circulating water bath at 30°C, well above the phase transition temperature of DMPC. The data were reduced to intensity I versus the reciprocal q space, where $q = 4\pi\sin(\theta)/\lambda$, 2θ is the scattering angle, and λ is the neutron wavelength. The reduction procedures, including normalization for incident flux spectrum, sample transmission, detector sensitivity, detector dark current, and azimuthal average, were performed with the facility-provided software.

Data Analysis

SANS data analysis was performed using BioXTAS Raw[23] and ATSAS[24]. Guinier analysis $I(q) = I(0)e^{-\frac{q^2R_g^2}{3}}$ provides the radius of gyration, *Rg*, of dilute homogeneous particles in solution[25]. For dilute particles with an extended long axis, e.g., rod-like shapes, a modified Guinier analysis $I(q) = \frac{1}{q}I(0)e^{-\frac{q^2R_c^2}{2}}$ can be performed to obtain the cross-section radius of gyration, *Rc* [26]. In the case of a homogeneous cylindrical rod, the cylinder radius *R* is related to *Rc* as $R=\sqrt{2}Rc$. The pair distance distribution function P(r) (PDDF) is calculated by an indirect Fourier transform of the scattering curve I(q) to provide model-free structural analysis in real space. It provides direct evidence of simple geometric shapes such as globular, sheet-like, or rod-like particles, as well as the maximum dimensions of the particle. For a special case such as a rod-like shape, the cross-sectional PDDF Pc(r) can be performed to provide more details on radical structure and maximum diameter Dc_max [27].

The power law fitting $I(q)=a \cdot q^m + b$ (*a* is a scale factor and *b* is background) provides a simple dimensionality factor for elucidating the basic geometry of a particle, such as sheet, rod, and fractal dimensions[28]. The fittings were performed in SASView package (sasview.org).

Ab initio Reconstruction

The scattering length density reconstruction from SANS data is performed by DENSS[29] in membrane mode with 20 reconstructions, subsequently averaged by default DENSS settings. The mean of correlation scores between them is 0.857 with standard deviation of 0.019. The resolution reported by DENSS is 28.8 Å. The resulting scattering length density is then scaled and normalized according the d54-DMPC hydrocarbon chain average NSLD (6.83×10^{-6} Å^{-2}), and buffer of 12% D_2O NSLD (0.29×10^{-6} Å^{-2}).

Results and Discussion

DIBMA in solution

To understand DIBMA structure in solution and to determine the neutron scattering CMP of DIBMA, we performed SANS experiments with 1 mM and 2.5 mM DIBMA in a 200 mM NaCl Tris buffer at different D_2O ratios (Fig. 1). From the linear fitting on $\sqrt{I}$ vs. D_2O ratio, the CMP of DIBMA was determined to be ~12% (v/v) D_2O (Fig. 2). The CMP is practically the same as the overall CMP of most protiated lipid molecules. [18] This similarity allows DIBMA to be used to assemble a membrane mimetic of uniform NSLD without special deuteration, which is tedious and prohibitively expensive in some cases. For example, to use MSP lipid nanodiscs, careful isotope labeling is required to produce a MSP in a D2O medium to match the CMP of the lipid so that the whole lipid nanodisc can be matched by a single CMP.

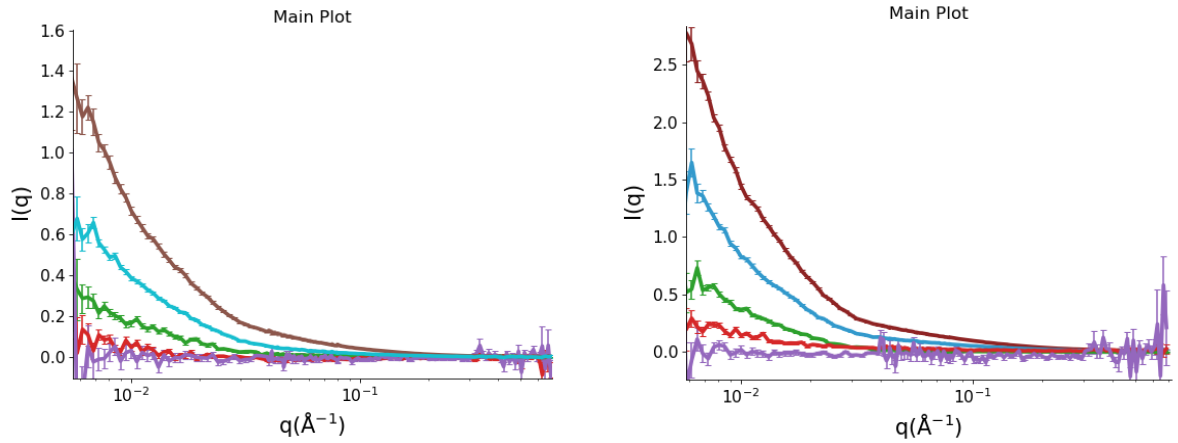

(a) **(b)**

Fig. 1 SANS of (a) 1mM and (b) 2.5mM DIBMA different D_2O ratios (from top to bottom: D_2O ratio (v/v) 96.5%, 73.0%, 50.0%, 31.0%, 15.0%), shown in linear-logarithmic plot for clarity.

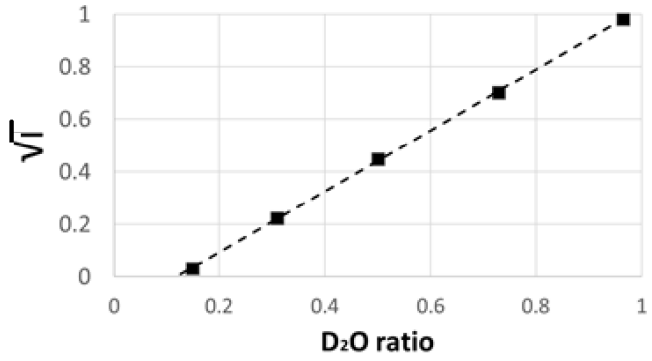

Figure 2. Determining the CMP of DIBMA with a contrast variation series at different D_2O ratios. The intercept to $\sqrt{I}=0$ with the linear regression (dashed line) on the data points $\sqrt{I}=1.157\times D_2O_{ratio}-0.137$ yields the CMP.

The SANS data at different D_2O ratios from both concentrations were similar (e.g., logarithmically plotted in Fig. 3a). They all show a power law feature close to a slope of −1, indicating extended structure [30] at different D2O ratios in both concentrations are similar. The slight deviation from −1 suggests some roughness on the rod-like particle[30].

From the PDDF, the particle Dmax as seen by neutron scattering was close to 700 Å . This revealed that the smaller rod-like DIBMA particles form larger-scale hierarchical structures showing the nature of a hyper-coiling polymer and polyelectrolyte. (Fig. 3) The smaller rod-like shape revealed from SAXS further organized into even larger elongated structures. In the modified Guinier analysis for the rod-like shape, the Rc was around 30 Å . Assuming a cylindrical rod, the cross-section radius R was ~50 Å.

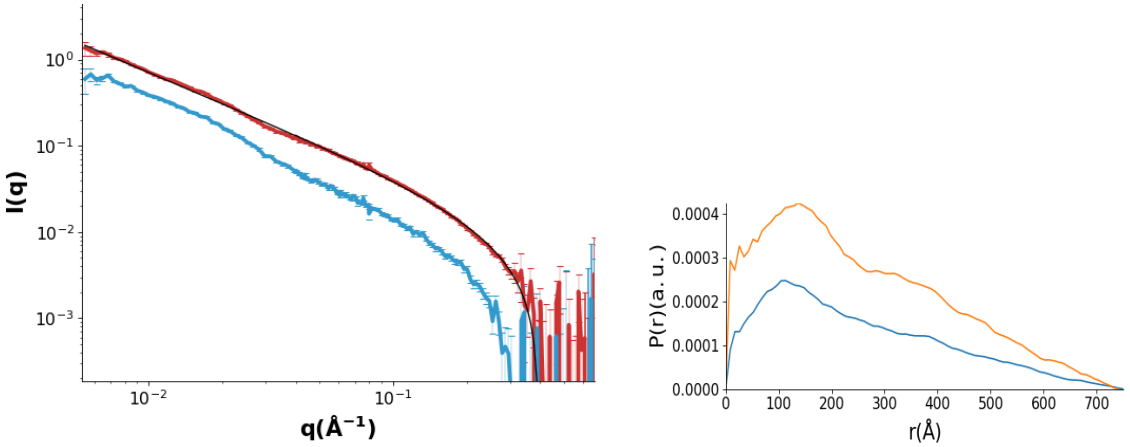

(a) (b)

Fig. 3 (a) SANS of DIBMA in 73% (blue) and 96.5% (red) D_2O are shown in logarithmic plot. The power law fitting is overlaid on the 96.5% D_2O as black. (b) P(r) of DIBMA SANS data in 73% (blue) and 96.5% (orange) D_2O

DIBMA Lipid Particle

Lipid-to-polymer ratio in forming DIBMALP: We observed that the addition of DIBMA to lipid vesicles caused the cloudy solution to become clearer as the ratio of DIBMA increased (lipid/polymer (w/w) 1.5, 1.25, 1.0, 0.75, 0.5, 0.25 [molar ratio ~22.0, 17.6, 13.2, 8.8, 4.4]) (an example of DMPC vesicles is shown in Fig. 4).

From the SAXS measured at Rigaku BioSAXS X-ray instrument, more details for the solution samples were attained (Fig. 5). At higher lipid-to-polymer ratios (e.g., lipid/polymer ~22 to 13.2 molar ratio), the slope of the curves at low q (below ~0.04 $Å^{-1}$) was close to –2, indicating a sheet-like structure of a 2-dimentional lipid vesicle bilayer. The first minimum and the peak near 0.1 $Å^{-1}$ suggest a typical lipid bilayer thickness, which is consistent with typical SAXS data from an intact lipid vesicle[31,32]. At lower lipid-to-polymer ratios, the slope was reduced, indicating the lipid vesicle dissolved in the increasing amounts of DIBMA polymer. This result shows the polymer solubilizes lipids in a concentration-dependent manner. A significant polymer-to-lipid ratio is needed to completely encapsulate the available lipids, resulting in lipid particles that are much smaller than lipid vesicles. We used therefore (DMPC/DIBMA = 10mM/5mM) for SANS study.

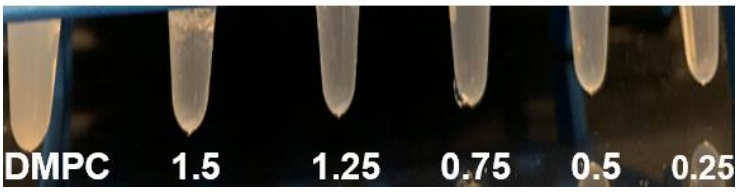

Fig. 4. The combination of DMPC vesicles and DIBMA Polymers at different lipid to polymer weight ratios

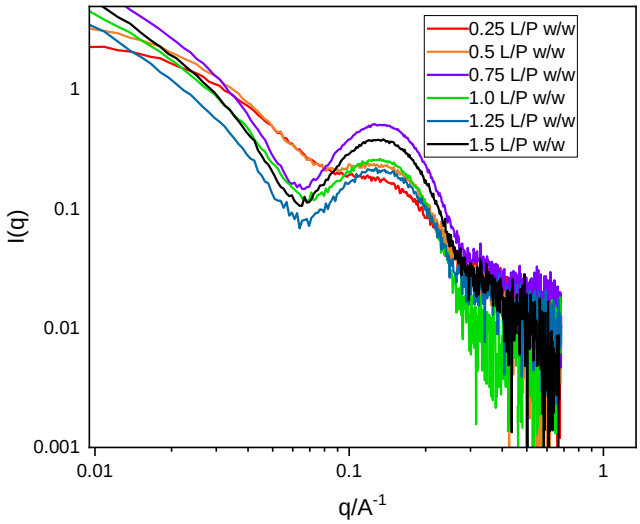

Fig. 5. SAXS Analysis of Scattering pattern showing the scattering intensity I as the function of scattering vector q for DIBMA lipid particles (DIBMALPs) at pH 7.5 with the DMPC/ DIBMA weight ratios of 0.25, 0.5, 0.75, 1, 1.25 and 1.5

As a "stealth" membrane mimic: From the DIBMA CMP we obtained, and the morphology of DIBMA with different lipid-to-polymer ratios, we went on to determine the lipid nanodisc structure and demonstrate the stealth lipid nanodisc. As shown by the purple curve in Fig. 6(a), the coherent SANS signal of DIBMALPs assembled from protiated lipids (DMPC/DIBMA = 10mM/5mM) is annihilated by a 12% D2O buffer, only showing featureless flat scattering, mostly from the incoherent scattering of hydrogen in the DIBMALPs. This result confirmed the whole DIBMALP can be contrast matched by using a 12% D2O buffer.

Additional curves in Fig. 6a also show SANS results for the DIBMALPs assembled from deuterated lipid d54-DMPC at various D_2O ratios. In this case, the CMP of the lipid was much higher than that of DIBMA, near 100% D_2O.[33] At D_2O ratios other than 12%, both polymer and lipid components showed a higher hierarchical structural organization of the polymer intertwined

with the nanodiscs. At 12% D_2O, the CMP of DIBMA, the scattering originated only from d54-DMPC. In other words, only the lipid compartment, especially the deuterated hydrocarbon chain region of the nanodisc is selectively observed. The thickness ~40A is consistent with a lipid hydrocarbon chain thickness.From the Guinier analysis and P(r), the Rg is ~19 Å and the D_{max} ~60 Å. The P(r) curve (Fig. 6a inset) indicates a quite symmetric and globular lipid particle presumably constrained by the polymer. We performed ab initio reconstruction on the SANS data only showing d54-DMPC nanodiscs (the red curve in Fig. 6a) with DENSS (Density from Solution Scattering program).[29] The resolved NSLD clearly shows an oblate discoidal shape (Fig. 6b) with high NSLD in the center matching the deuterated acyl chain of d54-DMPC (Fig. 6c). The DIBMA polymer surrounding the disk has been contrast matched completely (Fig. 6d).

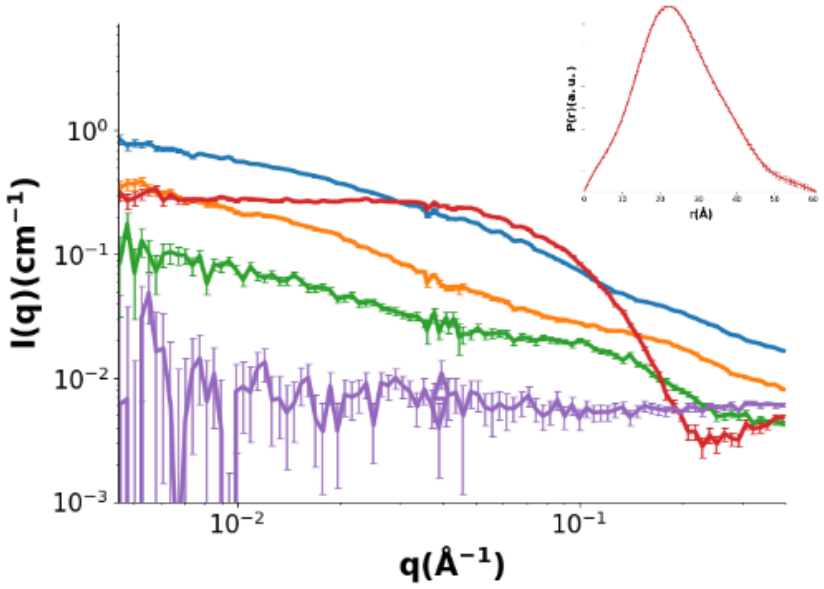

(a)

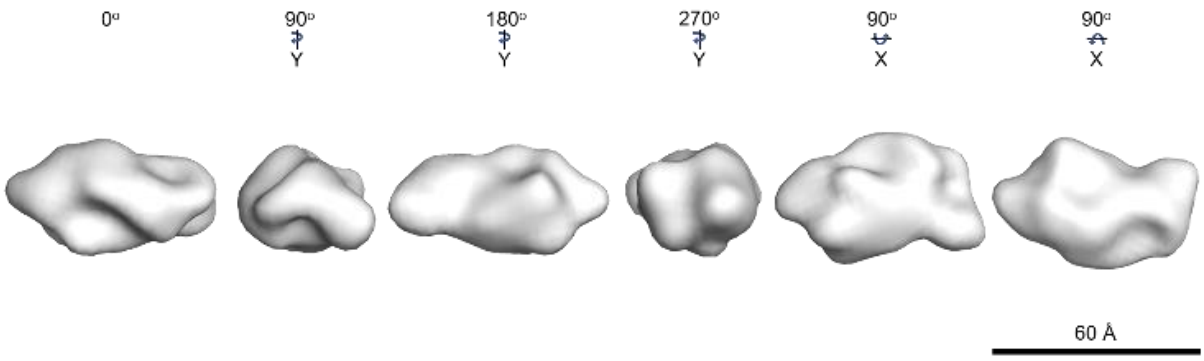

(b)

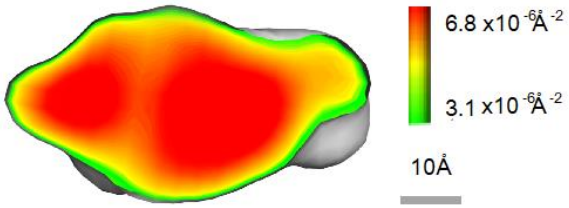

(c)

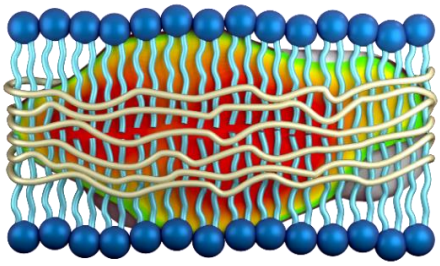

(d)

Figure 4. (a) SANS of DIBMALP composed of d54-DMPC measured at D_2O ratios of 12% (red), 50% (green), 75% (orange), 100% (blue). The inset is the P(r) for 12% data. SANS of DIBMALPs composed of protiated DMPC at 12% D_2O is shown in purple. (b) the ab initio shape from DENSS shown from different orientations. (c) A cross section of the NSLD density in the reconstructed result. (d) a cartoon overlaid with the NSLD to represent the structure.

Conclusions

We determined that the DIBMA CMP is practically the same as that of protiated lipids, while protein CMP is typically about ~42% D2O, presenting a natural contrast between DIBMALP and protein. Once DIBMA is used to extract and purify membrane protein with associated lipids, the samples can be used for an array of neutron scattering experiments for the selective study of protein without the interference of the membrane mimetic. This provides a straightforward approach without the need for isotope labeling, e.g., deuteration of polymer, lipids, or protein. This provide a solution for biomembranes that are not easily deuterated, which is one of the difficulties to study membrane protein under native lipid environment with SANS. Most SANS instrument can provides good signals for the contrast between lipid and protein even the incoherent background is high at ~12% D2O ratio. The compatibility of DIBMALP with other biophysical and structural techniques makes it possible to use the same samples for additional study.

References

(1) Uhlén, M.; Fagerberg, L.; Hallström, B. M.; Lindskog, C.; Oksvold, P.; Mardinoglu, A.; Sivertsson, Å.; Kampf, C.; Sjöstedt, E.; Asplund, A.; Olsson, I.; Edlund, K.; Lundberg, E.; Navani, S.; Szigyarto, C. A.-K.; Odeberg, J.; Djureinovic, D.; Takanen, J. O.; Hober, S.; Alm, T.; Edqvist, P.-H.; Berling, H.; Tegel, H.; Mulder, J.; Rockberg, J.; Nilsson, P.; Schwenk, J. M.; Hamsten, M.; von Feilitzen, K.; Forsberg, M.; Persson, L.; Johansson, F.; Zwahlen, M.; von Heijne, G.; Nielsen, J.; Pontén, F. Proteomics. Tissue-Based Map of the Human Proteome. *Science* **2015**, *347* (6220), 1260419. https://doi.org/10.1126/science.1260419.

(2) Overington, J. P.; Al-Lazikani, B.; Hopkins, A. L. How Many Drug Targets Are There? *Nat. Rev. Drug Discov.* **2006**, *5* (12), 993–996. https://doi.org/10.1038/nrd2199.

(3) Dürr, U. H. N.; Gildenberg, M.; Ramamoorthy, A. The Magic of Bicelles Lights Up Membrane Protein Structure. *Chem. Rev.* **2012**, *112* (11), 6054–6074. https://doi.org/10.1021/cr300061w.

(4) Giusti, F.; Rieger, J.; Catoire, L. J.; Qian, S.; Calabrese, A. N.; Watkinson, T. G.; Casiraghi, M.; Radford, S. E.; Ashcroft, A. E.; Popot, J.-L. Synthesis, Characterization and Applications of a Perdeuterated Amphipol. *J. Membr. Biol.* **2014**, *247* (9–10), 909–924. https://doi.org/10.1007/s00232-014-9656-x.

(5) Denisov, I. G.; Sligar, S. G. Nanodiscs for Structural and Functional Studies of Membrane Proteins. *Nat. Struct. Mol. Biol.* **2016**, *23* (6), 481–486. https://doi.org/10.1038/nsmb.3195.

(6) Knowles, T. J.; Finka, R.; Smith, C.; Lin, Y.-P.; Dafforn, T.; Overduin, M. Membrane Proteins Solubilized Intact in Lipid Containing Nanoparticles Bounded by Styrene Maleic Acid Copolymer. *J. Am. Chem. Soc.* **2009**, *131* (22), 7484–7485. https://doi.org/10.1021/ja810046q.

(7) Orwick, M. C.; Judge, P. J.; Procek, J.; Lindholm, L.; Graziadei, A.; Engel, A.; Gröbner, G.; Watts, A. Detergent-Free Formation and Physicochemical Characterization of Nanosized Lipid–Polymer Complexes: Lipodisq. *Angew. Chem. Int. Ed.* **2012**, *51* (19), 4653–4657. https://doi.org/10.1002/anie.201201355.

(8) Oluwole, A. O.; Danielczak, B.; Meister, A.; Babalola, J. O.; Vargas, C.; Keller, S. Solubilization of Membrane Proteins into Functional Lipid-Bilayer Nanodiscs Using a Diisobutylene/Maleic Acid Copolymer. *Angew. Chem. Int. Ed Engl.* **2017**, *56* (7), 1919–1924. https://doi.org/10.1002/anie.201610778.

(9) Hall, S. C. L.; Tognoloni, C.; Charlton, J.; Bragginton, É. C.; Rothnie, A. J.; Sridhar, P.; Wheatley, M.; Knowles, T. J.; Arnold, T.; Edler, K. J.; Dafforn, T. R. An Acid-Compatible Co-Polymer for the Solubilization of Membranes and Proteins into Lipid Bilayer-Containing Nanoparticles. *Nanoscale* **2018**, *10* (22), 10609–10619. https://doi.org/10.1039/C8NR01322E.

(10) Barniol-Xicota, M.; Verhelst, S. H. L. Stable and Functional Rhomboid Proteases in Lipid Nanodiscs by Using Diisobutylene/Maleic Acid Copolymers. *J. Am. Chem. Soc.* **2018**, *140* (44), 14557–14561. https://doi.org/10.1021/jacs.8b08441.

(11) Chill, J. H.; Qasim, A.; Sher, I.; Gross, R. NMR Perspectives of the KcsA Potassium Channel in the Membrane Environment. *Isr. J. Chem.* **2019**, *59* (11–12), 1001–1013. https://doi.org/10.1002/ijch.201900107.

(12) Cherepanov, D. A.; Brady, N. G.; Shelaev, I. V.; Nguyen, J.; Gostev, F. E.; Mamedov, M. D.; Nadtochenko, V. A.; Bruce, B. D. PSI-SMALP, a Detergent-Free Cyanobacterial Photosystem I, Reveals Faster Femtosecond Photochemistry. *Biophys. J.* **2019**. https://doi.org/10.1016/j.bpj.2019.11.3391.

(13) Bada Juarez, J. F.; Muñoz-García, J. C.; Inácio Dos Reis, R.; Henry, A.; McMillan, D.; Kriek, M.; Wood, M.; Vandenplas, C.; Sands, Z.; Castro, L.; Taylor, R.; Watts, A. Detergent-Free Extraction of a Functional Low-Expressing GPCR from a Human Cell Line. *Biochim. Biophys. Acta Biomembr.* **2019**, 183152. https://doi.org/10.1016/j.bbamem.2019.183152.

(14) Gulati, S.; Jamshad, M.; Knowles, T. J.; Morrison, K. A.; Downing, R.; Cant, N.; Collins, R.; Koenderink, J. B.; Ford, R. C.; Overduin, M.; Kerr, I. D.; Dafforn, T. R.; Rothnie, A. J. Detergent-Free Purification of ABC (ATP-Binding-Cassette) Transporters. *Biochem. J.* **2014**, *461* (2), 269–278. https://doi.org/10.1042/BJ20131477.

(15) Oluwole, A. O.; Klingler, J.; Danielczak, B.; Babalola, J. O.; Vargas, C.; Pabst, G.; Keller, S. Formation of Lipid-Bilayer Nanodiscs by Diisobutylene/Maleic Acid (DIBMA) Copolymer. *Langmuir* **2017**, *33* (50), 14378–14388. https://doi.org/10.1021/acs.langmuir.7b03742.

(16) Brady, N. G.; Qian, S.; Bruce, B. D. Analysis of Styrene Maleic Acid Alternating Copolymer Supramolecular Assemblies in Solution by Small Angle X-Ray Scattering. *Eur. Polym. J.* **2019**, *111*, 178–184. https://doi.org/10.1016/j.eurpolymj.2018.11.034.

(17) Heller, W. T. Small-Angle Neutron Scattering and Contrast Variation: A Powerful Combination for Studying Biological Structures. *Acta Crystallogr. D Biol. Crystallogr.* **2010**, *66* (11), 1213–1217. https://doi.org/10.1107/S0907444910017658.

(18) Zaccai, N. R.; Sandlin, C. W.; Hoopes, J. T.; Curtis, J. E.; Fleming, P. J.; Fleming, K. G.; Krueger, S. Deuterium Labeling Together with Contrast Variation Small-Angle Neutron Scattering Suggests How Skp Captures and Releases Unfolded Outer Membrane Proteins. *Methods Enzymol.* **2016**, *566*, 159–210. https://doi.org/10.1016/bs.mie.2015.06.041.

(19) Perera, S. M. D. C.; Chawla, U.; Shrestha, U. R.; Bhowmik, D.; Struts, A. V.; Qian, S.; Chu, X.-Q.; Brown, M. F. Small-Angle Neutron Scattering Reveals Energy Landscape for Rhodopsin

Photoactivation. *J. Phys. Chem. Lett.* **2018**, *9* (24), 7064–7071. https://doi.org/10.1021/acs.jpclett.8b03048.

(20) Gabel, F. Applications of SANS to Study Membrane Protein Systems. In *Biological Small Angle Scattering: Techniques, Strategies and Tips*; Chaudhuri, B., Muñoz, I. G., Qian, S., Urban, V. S., Eds.; Advances in Experimental Medicine and Biology; Springer: Singapore, 2017; pp 201–214. https://doi.org/10.1007/978-981-10-6038-0_12.

(21) Maric, S.; Skar-Gislinge, N.; Midtgaard, S.; Thygesen, M. B.; Schiller, J.; Frielinghaus, H.; Moulin, M.; Haertlein, M.; Forsyth, V. T.; Pomorski, T. G.; Arleth, L. Stealth Carriers for Low-Resolution Structure Determination of Membrane Proteins in Solution. *Acta Crystallogr. D Biol. Crystallogr.* **2014**, *70* (2), 317–328. https://doi.org/10.1107/S1399004713027466.

(22) Heller, W. T.; Cuneo, M.; Debeer-Schmitt, L.; Do, C.; He, L.; Heroux, L.; Littrell, K.; Pingali, S. V.; Qian, S.; Stanley, C.; Urban, V. S.; Wu, B.; Bras, W. The Suite of Small-Angle Neutron Scattering Instruments at Oak Ridge National Laboratory. *J. Appl. Crystallogr.* **2018**, *51* (2), 242–248. https://doi.org/10.1107/S1600576718001231.

(23) Hopkins, J. B.; Gillilan, R. E.; Skou, S. BioXTAS RAW: Improvements to a Free Open-Source Program for Small-Angle X-Ray Scattering Data Reduction and Analysis. *J. Appl. Crystallogr.* **2017**, *50* (5), 1545–1553. https://doi.org/10.1107/S1600576717011438.

(24) Franke, D.; Petoukhov, M. V.; Konarev, P. V.; Panjkovich, A.; Tuukkanen, A.; Mertens, H. D. T.; Kikhney, A. G.; Hajizadeh, N. R.; Franklin, J. M.; Jeffries, C. M.; Svergun, D. I. ATSAS 2.8: A Comprehensive Data Analysis Suite for Small-Angle Scattering from Macromolecular Solutions. *J. Appl. Crystallogr.* **2017**, *50* (4), 1212–1225. https://doi.org/10.1107/S1600576717007786.

(25) Guinier, A.; Fournet, G. *Small-Angle Scattering of X-Rays*; Wiley, 1955.

(26) Glatter, O. Evaluation of Small-angle Scattering Data from Lamellar and Cylindrical Particles by the Indirect Transformation Method. *J. Appl. Crystallogr.* **1980**, *13* (6), 577–584. https://doi.org/10.1107/S0021889880012794.

(27) *Scattering Methods and Their Application in Colloid and Interface Science*; Elsevier, 2018. https://doi.org/10.1016/C2016-0-04640-5.

(28) Beaucage, G.; Schaefer, D. W. Structural Studies of Complex Systems Using Small-Angle Scattering: A Unified Guinier/Power-Law Approach. *J. Non-Cryst. Solids* **1994**, *172–174*, 797–805. https://doi.org/10.1016/0022-3093(94)90581-9.

(29) Grant, T. D. *Ab Initio* Electron Density Determination Directly from Solution Scattering Data. *Nat. Methods* **2018**, *15* (3), 191–193. https://doi.org/10.1038/nmeth.4581.

(30) Teixeira, J. Small-Angle Scattering by Fractal Systems. *J. Appl. Crystallogr.* **1988**, *21* (6), 781–785. https://doi.org/10.1107/S0021889888000263.

(31) Graziano, V.; Miller, L.; Yang, L. Interpretation of Solution Scattering Data from Lipid Nanodiscs. *J. Appl. Crystallogr.* **2018**, *51* (Pt 1), 157–166. https://doi.org/10.1107/S1600576717018441.

(32) Pan, J.; Heberle, F. A.; Tristram-Nagle, S.; Szymanski, M.; Koepfinger, M.; Katsaras, J.; Kučerka, N. Molecular Structures of Fluid Phase Phosphatidylglycerol Bilayers as Determined by Small Angle Neutron and X-Ray Scattering. *Biochim. Biophys. Acta BBA - Biomembr.* **2012**, *1818* (9), 2135–2148. https://doi.org/10.1016/j.bbamem.2012.05.007.

(33) Qian, S.; Heller, W. T. Peptide-Induced Asymmetric Distribution of Charged Lipids in a Vesicle Bilayer Revealed by Small-Angle Neutron Scattering. *J. Phys. Chem. B* **2011**, *115* (32), 9831–9837. https://doi.org/10.1021/jp204045t.